Published for SISSA by Springer

Received: May 6, 2022
Revised: July 19, 2022
Accepted: July 25, 2022
Published: August 31, 2022

Phases of rotating baryonic matter: non-Abelian chiral soliton lattices, antiferro-isospin chains, and ferri/ferromagnetic magnetization

Minoru Eto,[a,b] **Kentaro Nishimura**[b,c,d] **and Muneto Nitta**[b,e]

[a] *Department of Physics, Yamagata University, Kojirakawa-machi 1-4-12, Yamagata, Yamagata 990-8560, Japan*
[b] *Research and Education Center for Natural Sciences, Keio University, 4-1-1 Hiyoshi, Yokohama, Kanagawa 223-8521, Japan*
[c] *Department of Physics, Keio University, 3-14-1 Hiyoshi, Yokohama, Kanagawa 223-8522, Japan*
[d] *KEK Theory Center, Tsukuba 305-0801, Japan*
[e] *Department of Physics, Keio University, 4-1-1 Hiyoshi, Yokohama, Kanagawa 223-8521, Japan*

E-mail: meto@sci.kj.yamagata-u.ac.jp, nishiken@post.kek.jp, nitta@phys-h.keio.ac.jp

Abstract: A chiral soliton lattice (CSL), proposed as the ground state of rotating baryonic matter at a finite density, is shown to be unstable in a large parameter region for two flavors owing to pion condensations, leading to two types of non-Abelian (NA) CSL phases (dimer and deconfining phases). We determine the phase diagram where the dimer phase meets the other phases and QCD vacuum at three tricritical points. The critical angular velocity of NA-CSLs is lower than that of η-CSL. Each NA soliton carries an isospin, and an antiferro-isospin chain is formed leading to gapless isospinons. The anomalous coupling to the magnetic field makes the NA-CSL (η-CSL) ferrimagnetic (ferromagnetic).

Keywords: Phase Diagram or Equation of State, Topological States of Matter, Effective Field Theories of QCD

ArXiv ePrint: 2112.01381

https://doi.org/10.1007/JHEP08(2022)305

JHEP08(2022)305

Contents

1 Introduction

Determination of the quantum chromodynamics (QCD) phase diagram under extreme conditions, such as at finite temperature and/or density, is a crucial problem in elementary particle physics, nuclear physics, and astrophysics. It has been reported that quark-gluon plasmas produced in non-central heavy-ion collision experiments at the Relativistic Heavy Ion Collider (RHIC) have the largest vorticity observed thus far, of the order of 10^{22}/s [1, 2]. Thus, rotating QCD matter has received significant attention in recent years. Moreover, recent developments in neutron star observations, such as the Laser Interferometer Gravitational-wave Observatory (LIGO) for the observation of gravitational waves from a neutron star [3, 4] and the Neutron star Interior Composition Explorer (NICER) mission [5, 6] may reveal states of QCD matter realized in rapidly rotating neutron stars. Therefore, it is crucial to investigate the effects of rotation on QCD matter. These effects have been theoretically studied by several researchers [7–18]; in particular, it has been predicted that due to the chiral vortical effect (CVE) [19–24], baryonic matter under rapid rotation exhibits a chiral soliton lattice (CSL), which is a periodic array of topological solitons that spontaneously break a translational symmetry [17, 18]. Similar CSLs also appear in QCD under an external magnetic field [25–28] and thermal fluctuation [29–31] (see also [32–34]). More generally, CSLs universally appear in various condensed matter systems; a partially twisted coherent spin structure in chiral magnets is realized as a

JHEP08(2022)305

CSL [35, 36]. Notably, as an important nanotechnological application, information processing using CSL has the potential to improve the performance of magnetic memory storage devices and magnetic sensors [37]. Formation of CSLs through quantum mechanical tunneling was recently proposed [38, 39].

In this paper, the phase diagram of rotating QCD matter is determined with two-flavor quarks at a finite baryon chemical potential, indicating that the ground state of the QCD at finite density under sufficiently fast rotation is a novel inhomogeneous state, called a *non-Abelian (NA) CSL*. We note that the conventional CSL of η mesons (η' for three flavors) [17, 18], referred to as the η-CSL, is unstable against pion fluctuations, leading to spatially modulated pion condensations in a large parameter region. In addition to the usual phonon, the vector $\mathrm{SU}(2)_{\mathrm{V}}$ symmetry is also spontaneously broken around each constituent soliton, resulting in the localization of S^2 NA Nambu-Goldstone (NG) modes (an isospin), and thus named it an NA chiral soliton (CS) [40, 41]. The NA-CSL phase can be further divided into two phases: the dimer phase, where the two solitons form a dimer molecule of a soliton pair with opposite isospins, and the deconfining phase, where the two solitons repel each other completely, thus forming an equally-separated opposite-isospin soliton lattice. Furthermore, gapless NG modes "isospinons" propagate along the lattice direction, analogous to magnons in antiferromagnets. The CSL also shows magnetization due to the anomalous coupling of the π_0 meson to the magnetic field [25, 42, 43], and NA-CSL (η-CSL) is ferrimagnetic (ferromagnetic). We also discuss the possibility of finding the CSL in future low-energy heavy ion collision experiments.

2 The model

The two-flavor chiral Lagrangian of the η meson and pions $\vec{\pi}$ is given by

$$\begin{aligned}\mathcal{L} = &\frac{\Omega\mu_{\mathrm{B}}^2}{2\pi^2 N_c}\partial_z\frac{\eta}{f_\eta} + \frac{f_\pi^2}{4}g^{\mu\nu}\,\mathrm{tr}\left[\partial_\mu\Sigma\partial_\nu\Sigma^\dagger\right] + \frac{1}{2}g^{\mu\nu}\partial_\mu\eta\partial_\nu\eta \\ &+\left\{\frac{A}{2}\left(\det U - 1\right) + \frac{B}{2}\,\mathrm{Tr}\left[M(U-1)\right] + \mathrm{h.c.}\right\},\end{aligned} \tag{2.1}$$

where the U(2) field U is decomposed as

$$U = \Sigma\exp(i\eta/f_\eta), \tag{2.2}$$

with the SU(2) element

$$\Sigma = \exp(i\tau_A\pi_A/f_\pi), \tag{2.3}$$

(τ_A is Pauli's matrix $A = 1, 2, 3$), and $f_{\pi,\eta}$ are the decay constants of the pions and η meson. This system is rotated about the z-axis with angular velocity Ω. The rotation effect is considered in the metric tensor $g_{\mu\nu}$, and the first term μ_{B} (baryon chemical potential) reproduces the CVE in terms of the η meson.[1] The fourth and fifth terms reflect the QCD anomaly and quark mass term, yielding masses to the η and $\vec{\pi}$, respectively. It is assumed

[1] See appendix A for details on the CVE term.

JHEP08(2022)305

that $M = m\mathbf{1}_2$, which is valid for $\mu_{\rm B} \gg m_{\rm u,d}$. The Lagrangian is invariant under the vector symmetry $\mathrm{SU(2)_V}$: $U \to VUV^\dagger$, while the $\mathrm{U(1)_A}$ (chiral) symmetry is explicitly broken by the anomaly (mass) term.

The Lagrangian (2.1) is valid as far as the chiral symmetry is spontaneously broken. When $\mu_{\rm B}$ becomes a large unknown value ($\gg 1\,\mathrm{GeV}$) at which the phase transits to the two-flavor color-superconducting (2SC) quark matter [44–47], the chiral symmetry is unbroken and the Lagrangian is not valid. In the region between $\mu_{\rm B} \sim m_{\rm N}$ (the nucleon mass $\sim 1\,\mathrm{GeV}$) and 2SC, we have to consider coupling between mesons in eq. (2.1) and nuclear matter, which we do not do in this paper.

This study considers an array of solitons, namely CSLs, extending along the rotation axis z. For this purpose, it is assumed that the fields depend on the z-coordinate alone, without loss of generality, and $\pi_{1,2} = 0$ is set for constructing ground states. Furthermore, dimensionless fields $\phi_{0,3}$ defined by $\phi_0 = \eta/f_\eta$ and $\phi_3 = \pi_3/f_\pi$ are largely used, along with the dimensionless variables $\zeta = \sqrt{C}z/f_\eta$, $\epsilon \equiv 1 - (f_\pi/f_\eta)^2$, and

$$S = \Omega/(2\pi^2 N_c f_\eta \mu_{\rm B}^{-2}\sqrt{C}) \tag{2.4}$$

with $C = \sqrt{A^2 + (4mB)^2}$. Then, the reduced Hamiltonian density is

$$\frac{\mathcal{H}}{C} = \frac{1-\epsilon}{2}\phi_3'^2 + \frac{1}{2}\phi_0'^2 + \sin\beta(1-\cos 2\phi_0) + \cos\beta\,(1-\cos\phi_0\cos\phi_3) - S\phi_0', \tag{2.5}$$

where A and B are parameterized by

$$\tan\beta \equiv A/(4mB). \tag{2.6}$$

Additionally, we have neglected the higher-order contributions of $\Omega/(4\pi f_{\pi,\eta})$ [17, 18]. It can be observed that the independent parameters are ϵ, β, and S. The potential minimum is unique and is $U = \mathbf{1}_2$, which corresponds to $(\phi_0, \phi_3) = (2m\pi, 2n\pi)$ and $((2m+1)\pi, (2n+1)\pi)$, with $m, n \in \mathbb{Z}$ in the ϕ_0-ϕ_3 plane.[2]

3 Linear instability of η-CSL

Recently, ref. [18] reported that when the rotation speed S is sufficiently large, η-CSL, which straightly connects the infinite discrete vacua $(\phi_0, \phi_3) = (2\pi n, 0)$ (where ϕ_0 is a monotonically increasing step-function-like configuration, whereas ϕ_3 vanishes everywhere), becomes the ground state owing to the CVE term.

First, the linear (in)stability of the η-CSL, which was not studied in ref. [18], is clarified. Let $\bar{\phi}_0(\zeta)$ be the η-CSL background solution with lattice size ℓ, where $\bar{\phi}_A(\zeta) = 0$ $(A = 1, 2, 3)$. The black curves in figure 1 represent a typical configuration (with a single period) for $(\beta, \epsilon, \ell) = (\pi/16, 0.1, 15)$. All fields are perturbed as $\phi_0 = \bar{\phi}_0 + \delta\phi_0$ and $\phi_A = \delta\phi_A$ and are not mixed in the linearized equations of motion (EOMs).[3] Clearly, no instability arises in the $\delta\phi_0$ sector, and a tachyonic instability may exist in the $\delta\phi_A$ sector. It is found

[2] See appendix A for the potential and vacuum with various parameter choices.
[3] See appendix B for the derivations of the linearized EOMs for the η-CSL.

JHEP08(2022)305

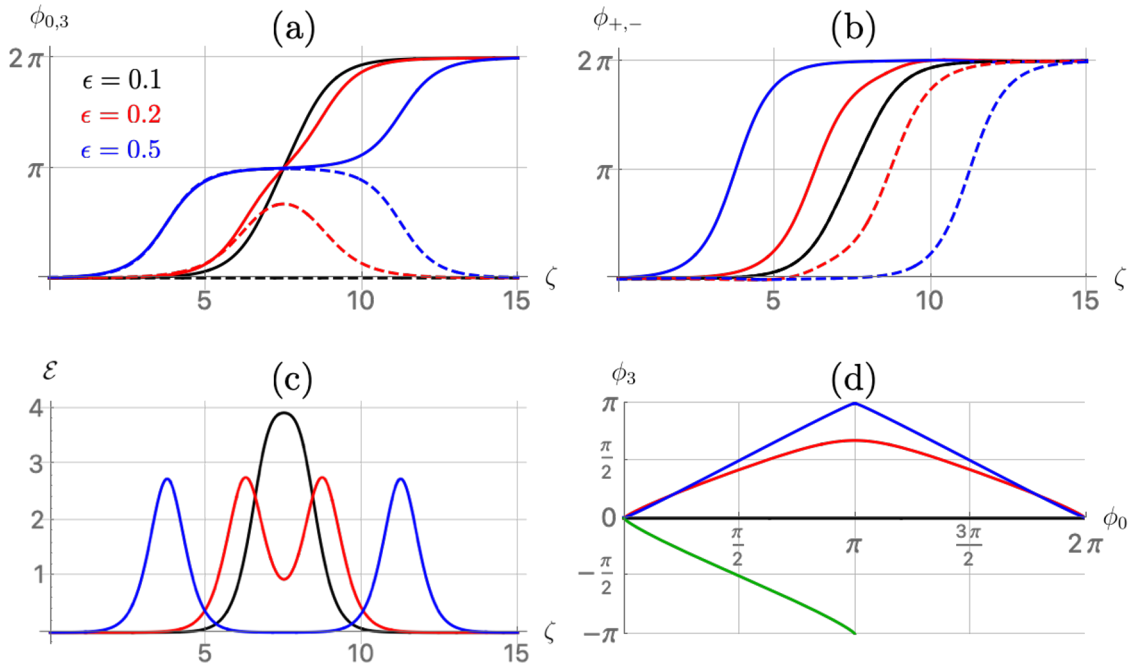

Figure 1. Numerical solutions of CSLs (shown within one period) for $\beta = \pi/16$ and $\ell = 15$. The black, red, and blue curves correspond to $\epsilon = 0.1$ (η-CSL), 0.2 (dimer NA-CSL), and 0.5 (deconfined NA-CSL), respectively. The solid (dashed) curves show (a) ϕ_0 (ϕ_3) and (b) ϕ_+ (ϕ_-). (c) Energy densities without the CVE term. (d) Solutions plotted in the ϕ_0-ϕ_3 plane. The green curve indicates the single d-CS with $\epsilon = 0.2$.

that η-CSL is always stable for $\epsilon < 0$ ($f_\eta < f_\pi$), whereas it can be unstable for $\epsilon > 0$ ($f_\eta > f_\pi$).[4] Figure 2(a) shows stable/unstable regions of η-CSL in the parameter plane ℓ-ϵ. Each curve shows a boundary above (below) which the lowest energy eigenvalue is negative (positive), leading to its instability (stability) for fixed β values. The curves starting from $(\ell, \epsilon) = (0, 0)$ monotonically increase for small ℓ and tend to the critical value ϵ_1 when the period ℓ exceeds the typical size of a single soliton, which is of order one with respect to the dimensionless coordinate ζ. The η-CSL is reduced to a single η-CS for a large period $\ell = \infty$. The ϵ_1 value shown in figure 2(b) is defined as the border of the linear stability of a single η-CS. For a given pair of β and ϵ, if $\epsilon > \epsilon_1$, there exist no stable η-CSLs, and if $\epsilon < \epsilon_1$, η-CSL is stable only when ℓ is larger than the critical value $\ell_1 = \ell(\beta, \epsilon)$ on the boundary; however, it is unstable below ℓ_1, see figure 2(a) for $\ell_1(\pi/16, 0.1)$ as an example. Namely, a sparse (dense) η-CSL tends to be (un)stable.

Single-CS and critical angular velocity. Here, by examining a single CS, the critical angular velocity S_c (dimensionless) is determined, above which the CSL becomes the ground state.

First, consider a single η-CS ($\phi_3 = 0$) that connects $(\phi_0, \phi_3) = (0, 0)$ and $(2\pi, 0)$ as $\zeta = -\infty$ and $+\infty$ (see the black segment in figure 1(d)). Because the endpoints are

[4] In the three-flavor case [18], the ratio $f_{\eta'}/f_\pi$ for the vacuum values is estimated as ≈ 1.1, implying that $\epsilon \approx 0.17 > 0$.

JHEP08(2022)305

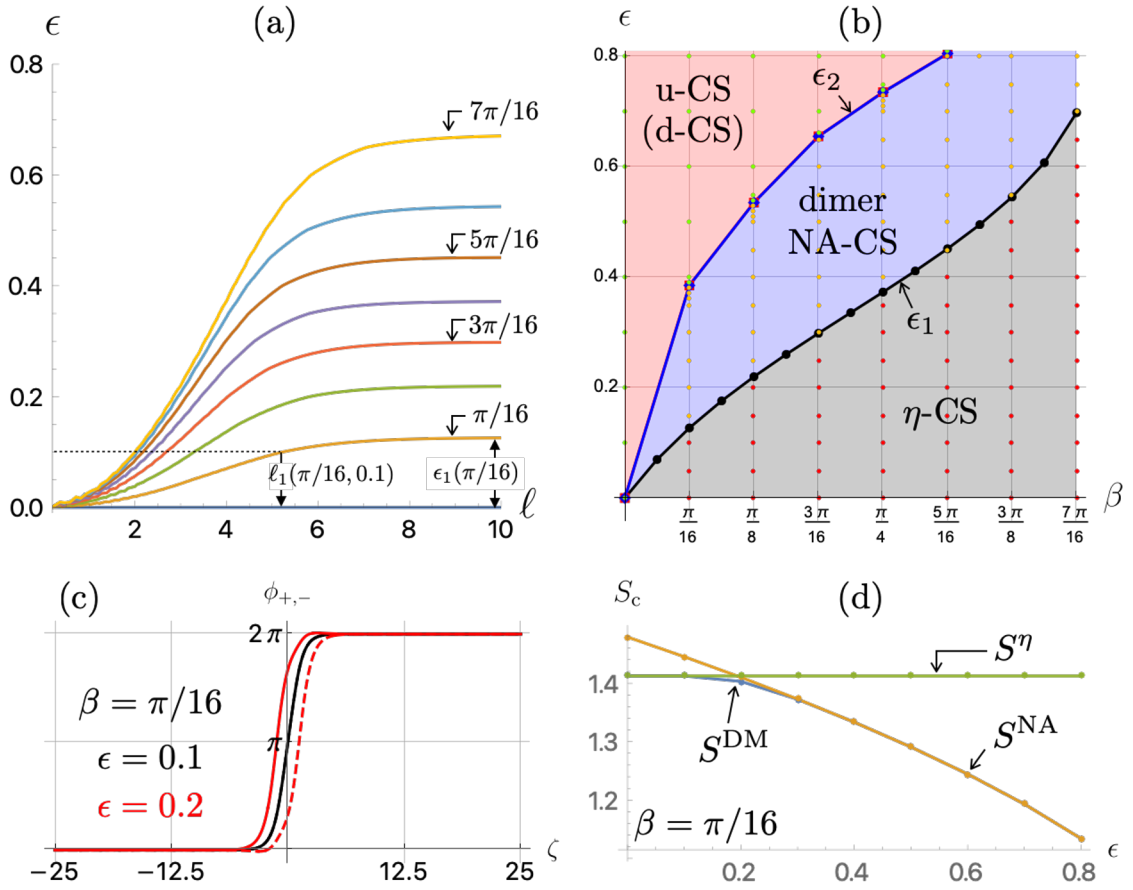

Figure 2. (a) Linear stability of the η-CSL in the ℓ-ϵ plane. It is unstable above each curve with $\beta = 0 - 7\pi/16$. (b) Phase diagram of a single CS. The black and blue dotted lines show ϵ_1 and ϵ_2, respectively. (c) The solid (dashed) curve corresponds to ϕ_+ (ϕ_-). The black (red) curves are as follows: For η-CS of $\epsilon = 0.1$ (dimer NA-CS of $\epsilon = 0.2$). $\beta = \pi/16$. (d) Three critical velocities S^η, $S^{\rm NA}$, and $S^{\rm DM}$ are shown for $\beta = \pi/16$.

identical ($U = \mathbf{1}_2$), the segment can be identified with a loop in the field space. The loop is topologically nontrivial because it winds once around $\mathrm{U}(1) \subset \mathrm{U}(2)$. The solution is easily obtained because $\phi_3 = 0$ can be consistently set, following which EOM reduces to the well-known double sine-Gordon equation. Ref. [18] reports that the tension of η-CS (integration of $\mathcal{H}$ without the CVE term for $-\infty \le \zeta \le \infty$) is given by

$$T^\eta(\beta) = 4\int_0^\pi \sqrt{\sin\beta \sin^2\theta + \cos\beta \sin^2\frac{\theta}{2}}\, d\theta, \tag{3.1}$$

and the total tension including the CVE term is $M^\eta = T^\eta - 2\pi S$. Because of the CVE term, M^η decreases as S increases. When S is equal to the critical value $S^\eta = T^\eta/2\pi$, the single η-CS is degenerate in energy with the homogeneous QCD vacuum. Note that the $\mathrm{U}(2)$ field U is proportional to $\mathbf{1}_2$; therefore, $\mathrm{SU}(2)_{\rm V}$ is unbroken everywhere.

There exists another loop topologically distinguishable from a single η-CS. It connects $(0, 0)$ and (π, π) at $\zeta = -\infty$ and $+\infty$; thus, it corresponds to a diagonal curve between

JHEP08(2022)305

$(0,0)$ and (π,π), as shown in figure 1(d). This winds only a half around U(1). In this sense, it is the minimum loop among topologically nontrivial loops. This is possible owing to the $\mathbb{Z}_2$ quotient of $\mathrm{U}(2) \simeq [\mathrm{U}(1) \times \mathrm{SU}(2)]/\mathbb{Z}_2$; specifically, $e^{i\phi_0} = -1$ and $\Sigma = e^{i\pi\tau_3} = -\mathbf{1}_2$ give $U = \mathbf{1}_2$ at (π,π). As ϕ_3 is no longer zero, the corresponding soliton is a NA-CS [40, 41]. Indeed, an important feature specific to NA-CS is that it possesses NA moduli; it passes the point $(\pi/2,\pi/2)$, namely $U = -\tau_3$, where $\mathrm{SU}(2)_\mathrm{V}$ is spontaneously broken into its subgroup U(1). Therefore, the NG modes $\mathrm{SU}(2)_\mathrm{V}/\mathrm{U}(1) \simeq S^2$ appear locally around the NA-CS, endowing it with an isospin.

Consider this NA-CS as the north pole of the moduli space S^2. By applying the $\mathrm{SU}(2)_\mathrm{V}$ transformation to the north pole solution, a continuous family of solutions having the same tension is obtained. In the ϕ_0-ϕ_3 plane, the NA-CS connecting $(0,0)$ and $(\pi,-\pi)$, (corresponding to the south pole) can be observed (see the green curve in figure 1(d)). The former is referred to as u-CS and the latter as d-CS. All other solutions connect two points outside this plane. Let T^NA be the tension of the single NA-CS (obtained from $\mathcal{H}$ with the CVE term excluded). It is dependent on both β and ϵ and can only be computed numerically. The total tension, including the CVE term, is $M^\mathrm{NA} = T^\mathrm{NA} - \pi S$. Note that the second term is πS and not $2\pi S$ because ϕ_0 increases by π for NA-CS. Hence, the other critical angular velocity is obtained as $S^\mathrm{NA} = T^\mathrm{NA}/\pi$.

The final possibility is a dimer state, i. e. a pair of the u-CS connecting $(0,0)$ and (π,π) and d-CS connecting (π,π) and $(2\pi,0)$. This pair is topologically equivalent to a single η-CS. Whether they split or combine is determined by their interactions, depending on the parameters ϵ and β. Qualitatively, it is found that a positive (negative) ϵ value induces repulsion (attraction) between them, while a non-zero β value yields an attractive interaction. When the repulsive and attractive interactions balance, u- and d-CSs are bound to form a dimer with a finite distance. Let T^DM be the tension of the dimer obtained from $\mathcal{H}$ without the CVE term. Then, the critical angular velocity is given by $S^\mathrm{DM} = T^\mathrm{DM}/2\pi$. However, when the attractive force dominates, u- and d-CSs coalesce, reducing to a single η-CS. When the repulsive force dominates, they repel each other, and the most stable state is (infinitely separated) single NA-CSs.

Thus, three critical velocities were found: S^η, S^NA, and S^DM. The actual critical angular velocity is given by $S_\mathrm{c}(\beta,\epsilon) \equiv \min\left[S^\eta, S^\mathrm{NA}, S^\mathrm{DM}\right]$. The CS that is realized depends on β and ϵ.

The existence of all three cases is confirmed by numerically solving EOMs.[5] We apply a relaxation method with an initial configuration of a pair of separated u- and d-CSs. Plotting $\phi_\pm = \phi_0 \pm \phi_3$ helps to determine whether the solution is an η-CS or NA-CS. This is because a 2π-jumping soliton of ϕ_+ (ϕ_-) represents u-(d-)CS. Hence, when the solution has ϕ_+ and ϕ_-, which lie on top of each other, it can be concluded that the ground state is η-CS; otherwise, it is NA-CS. Figure 2(c) shows examples of η-CS and NA-CS. Then, a dimer and a pair of repelling u- and d-CSs were further distinguished by observing their separation. The result was superposed on figure 2(b). The red dots, which represent η-CS, are all below ϵ_1, indicating a consistent relationship between the linear stability and relaxation analysis. The yellow dots correspond to dimers, and the green dots represent

[5] See appendix A for the derivation of the EOMs.

JHEP08(2022)305

a repelling pair of u- and d-CSs. ϵ_1, which was originally introduced as the border of the linear stability of a single η-CS, is now identified with the boundary between a single η-CS and the dimer of u- and d-CSs. Furthermore, another critical value is found, ϵ_2 (yellow curve with squares), which is the boundary between a dimer and a single NA-CS.

Figure 2(d) shows the critical angular velocities for $\beta = \pi/16$ and $\epsilon \geq 0$. It was found that $S_{\rm c} = S^{\eta}$ for $\epsilon < \epsilon_1$, $S_{\rm c} = S^{\rm DM}$ for $\epsilon_1 < \epsilon < \epsilon_2$, and $S_{\rm c} = S^{\rm NA}$ for $\epsilon > \epsilon_2$. It should be noted that when NA-CS is the ground state, irrespective of whether it is a dimer or single NA-CS, $S_{\rm c}$ is lower than that of the η-CS found in ref. [18]. The η-CS and dimer are topologically indistinguishable. However, $\mathrm{SU}(2)_{\rm V}$ is unbroken for the η-CS and is spontaneously broken into $\mathrm{U}(1)_{\rm V}$ for the NA-CS. The number of NG modes is 1 (translation) for the η-CS and $1+2$ (translation and isospin) for the NA-CS.

4 CSL for $S \geq S_{\rm c}$

When S exceeds $S_{\rm c}$, a periodic array of CSs appears with lattice spacing ℓ. Again, EOMs were numerically solved without assuming $\phi_3 = 0$. However, in this case, periodic boundary conditions $\phi_0(\zeta) = \phi_0(\zeta + \ell) + 2\pi$ and $\phi_3'(\zeta) = \phi_3'(\zeta + \ell)$ are imposed. Thus, ℓ is included as a free parameter in addition to β, ϵ, and S, and determined as follows: As S appears only through the topological term, it does not appear in EOMs. Hence, the EOMs are first solved for various values of ℓ by setting specific values for β and ϵ. Then the tension

$$M(\ell, S; \epsilon, \beta) = \int_0^{\ell} C^{-1}\mathcal{H}\, d\zeta = T(\ell; \epsilon, \beta) - 2\pi S, \tag{4.1}$$

is calculated, where T is the integration of the right-hand side of $\mathcal{H}$, with the exception of the last term. Finally, S is set, M is regarded as a function of ℓ, and a value of ℓ that minimizes the averaged mass $\bar{M}(\ell) \equiv M(\ell; \epsilon, \beta, S)/\ell$ is considered. Thus, $\ell(S; \beta, \epsilon)$ is obtained as a function of S for specific β and ϵ values. See figure 3(a) for an example of $(\beta, \epsilon) = (\pi/16, 0.3)$.

By repeating the above procedure for various (ϵ, β), the CSL phases could be clarified. Similar to the single CSs explained above, CSLs are classified into η-CSLs or NA-CSLs. In a single CSL period, there exists a pair of u- and d-CSs. In η-CSLs, u- and d-CSs are confined, whereas they are split for NA-CSLs. The latter is further classified based on whether u- and d-CSs are bound to form a dimer. Figure 1 shows examples of η-CSL (black for $\epsilon = 0.1$), dimer NA-CSL (red for $\epsilon = 0.2$), and deconfined NA-CSL (blue for $\epsilon = 0.5$) for $\beta = \pi/16$ and $\ell = 15$.[6] The following three phases can be defined:

(i) Confining phase: u- and d-CSLs are confined to form an η-CSL.

(ii) Dimer phase: u- and d-CSLs are confined and locally split to form a dimer.

(iii) Deconfining phase: u- and d-CSLs repel each other completely, thus forming an equally-separated up-and-down soliton lattice.

[6] See appendix A for the numerical solutions with various parameters.

JHEP08(2022)305

The phase that is realized depends not only on β and ϵ, but also on ℓ (or S from the relation $\ell(S)$). Figure 3(b) shows a distance d between u- and d-CSs in one period for $\beta = \pi/16$ and $\epsilon = 0.1$, 0.3, and 0.45. As mentioned previously, the interaction between u- and d-CSs originating from $\epsilon(> 0)$ is repulsive, and that from β is attractive. This explains the behavior of d at an asymptotically large period ℓ. The CSL at a large period ℓ is an η-CSL ($d = 0$) for $\epsilon = 0.1$ because the attractive force is dominant. In addition, it is a dimer NA-CSL for $\epsilon = 0.3$ because d tends to be constant, implying a dimer size for a large period ℓ. The separation d at $\epsilon = 0.45$ is on the line $d = \ell/2$, implying the u- and d-CSs are maximally (and thus equally) separated in one period ℓ, for which the CSL belongs to the deconfining phase. Note that these asymptotic behaviors are consistent with those depicted in figure 2(b), which represents a single η-CS/NA-CS ($\ell \to \infty$). As ℓ decreases, a dimer NA-CSL ($\epsilon = 0.3$) at an asymptotically large ℓ enters the deconfining phase. The transition point ℓ_2 can be understood as a point below which mutual influence between adjacent dimers becomes significant. Similarly, an η-CSL ($\epsilon = 0.1$) at an asymptotically large ℓ exhibits two successive transitions for a smaller ℓ. The first transition from the η-CSL to the dimer NA-CSL occurs at ℓ_1, which is in good agreement with the critical period separating stable/unstable η-CSLs obtained via linear stability analysis [see ℓ_1 values in figure 2(a) and 3(b)]. Subsequently, the second transition occurs at $\ell = \ell_2$ ($< \ell_1$) from the dimer to the deconfined NA-CSL.

Figure 3(c) shows the phase diagram in the ϵ-ℓ plane for $\epsilon > 0$ ($\epsilon < 0$ is uniformly within the confining phase). The curve ℓ_1 divides the confining and NA-CSL phases, and ℓ_2 further divides the NA-CSL into the dimer and deconfining phases. ℓ_1 and ℓ_2 meet at the critical point $(\epsilon_3, \ell_1(\epsilon_3))$. Figure 3(d) shows the phase diagram in the ϵ-S plane obtained by the relation $\ell(S)$; it is useful to observe the region around the curve corresponding to the critical velocity. The phase boundary between the QCD vacuum and the CSL phase represents the union of the bottom edges of the colored regions, where the two tricritical points $\epsilon = \epsilon_{1,2}$ can be found. The critical velocity S_c for the NA-CSLs is lower than the S^η value of the η-CSL for $\epsilon > \epsilon_1$; thus, it has higher potential for the discovery of a CSL in nature as compared to the η-CSL in ref. [18]. The dimer phase is found to meet two phases among the deconfining/confining phases and the QCD vacuum at three tricritical points $\epsilon_{1,2,3}$.

All the boundaries are phase boundaries, since each phase has a distinct symmetry. Symmetries of confining, dimer, and deconfining phases are $\mathrm{SU}(2)_V \times T(\ell)$, $\mathrm{U}(1) \times T(\ell)$, and $\mathrm{U}(1) \times \tilde{T}(\ell/2)$, respectively, where $T(a)$ denotes a translation along the ζ-axis by a, while $\tilde{T}$ is a simultaneous action of a translation $T(\ell/2)$ and $i\tau_2 \in \mathrm{SU}(2)_V$ which exchanges u- and d-CSs.

5 Isospinons

Here, the gapless NG modes propagating along the lattice called isospinons (analogous to magnons propagating along an antiferromagnetic spin chain) are discussed. Either in the dimer or deconfining phase, u- and d-CSs appear sequentially, where the isospin moduli of the former (latter) are directed to the north (south) pole of S^2. Therefore, the isospins of

JHEP08(2022)305

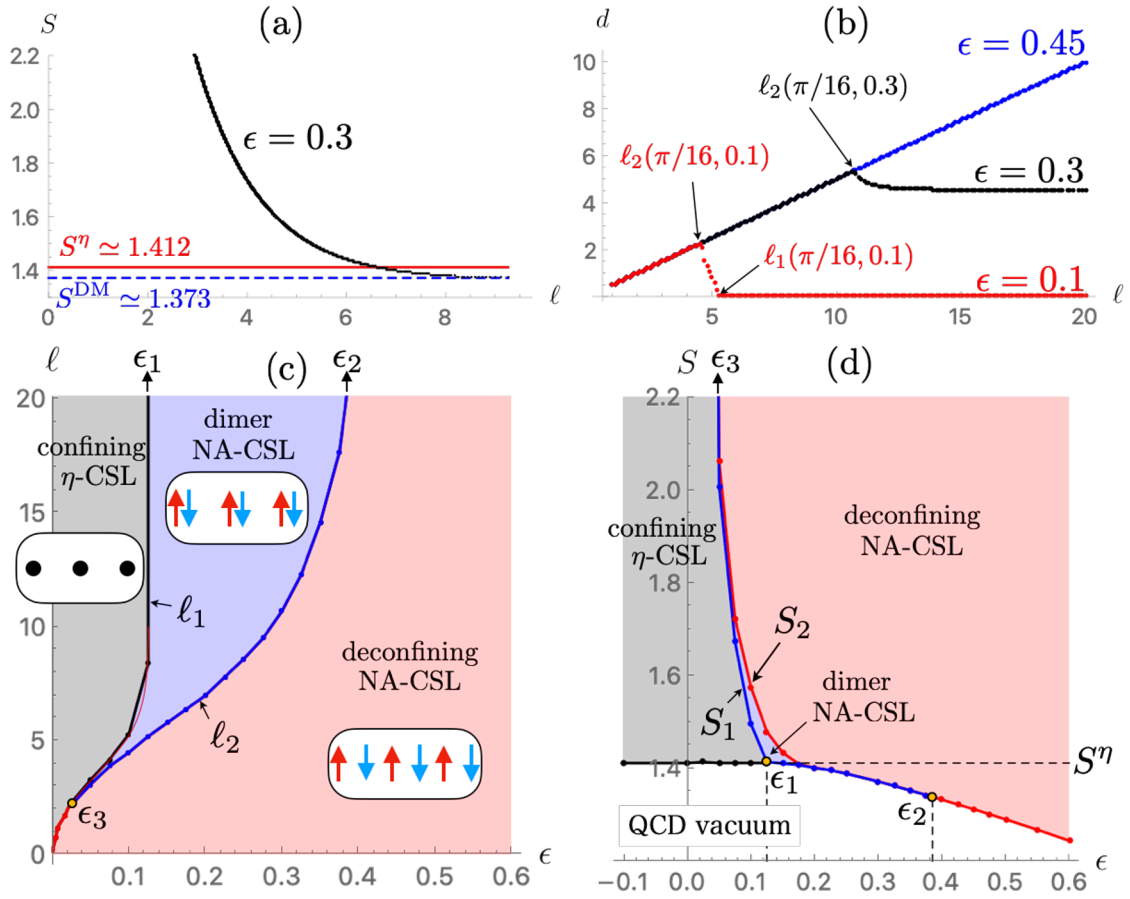

Figure 3. CSLs for $\beta = \pi/16$. (a) Relation $\ell(S)$ is shown for $\epsilon = 0.3$. ℓ diverges at $S = S^{\rm DM}$ ($< S^\eta$). (b) Distance d between u- and d-CSs is shown as a function of ℓ for $\epsilon = 0.1$, 0.3, and 0.45. Points on the line $d = \ell/2$ correspond to the deconfined NA-CSL, the dimer NA-CSL ($d \neq 0$), or the η-CSL ($d = 0$). (c) CSL phase diagram in the ϵ-ℓ plane. The array of arrows represents the antiferro-isospin chain of the NA-CSL, while that of black dots represents the η-CSL (isoscalar). The thin-red-solid curve corresponds to the border of the η-CSL linear stability for $\beta = \pi/16$, given in figure 2(a). (d) CSL phase diagram in the ϵ-S plane. In (c) and (d), $\epsilon_{1,2,3}$ correspond to the three tricritical points.

neighboring NA-CSLs are antiparallel, and they are thus regarded as an antiferro-isospin chain. There exist massless NG modes (isospinons) associated with $\mathrm{SU}(2)_{\rm V} \to \mathrm{U}(1)$ propagating along the lattice. They can be found in small perturbations around the background NA-CSL: $\phi_a = \bar{\phi}_a + \delta\phi_a$ ($a = 0, 1, 2, 3$), where $\bar{\phi}_a$ represents the background solution.

For simplicity, the point $\beta = \epsilon = 0$ for which there is an available analytical solution is considered here:

$$\bar{\phi}_0 \pm \bar{\phi}_3 = 2\,\mathrm{am}\left(\frac{\zeta \mp d/2}{k}, k\right) + \pi, \quad \bar{\phi}_{1,2} = 0, \tag{5.1}$$

with d corresponding to the separation between u- and d-CSs. In addition to the translational NG mode (phonon), $\delta\phi^{(0)}_{0,3} \propto \bar{\phi}'_{0,3}$, there exist two gapless isospinons,

$$\delta\phi^{(0)}_1 \pm i\delta\phi^{(0)}_2 \propto e^{\mp i\bar{\phi}_3}\bar{\phi}'_0, \tag{5.2}$$

JHEP08(2022)305

which propagate along the u- and d-CSLs.[7, 8] The phonon and isospinon robustly exist because they are NG; they exist in NA-CSLs with generic β and ϵ values. In contrast, there is only one gapless mode, a phonon, on the η-CSL.

6 Rotation-induced ferro/ferrimagnetism

Finally, magnetizations appearing through another topological term under an external magnetic field $\boldsymbol{B}$ are shown: [25, 42, 43]:

$$\mathcal{L}_{\rm top} = \frac{q_{\rm u}\mu_{\rm B}}{4\pi^2}\nabla\phi_+ \cdot \boldsymbol{B} + \frac{q_{\rm d}\mu_{\rm B}}{4\pi^2}\nabla\phi_- \cdot \boldsymbol{B}. \tag{6.1}$$

From this, the magnetizations of the u-NA-CSs, d-NA-CSs, and η-CS are determined as

$$\boldsymbol{M}_{\rm u,d} = -\frac{q_{\rm u,d}\mu_{\rm B}}{4\pi^2}\nabla\phi_{+,-}\,, \quad \boldsymbol{M}_\eta = -\frac{1}{3}\frac{e\mu_{\rm B}}{4\pi^2}\nabla\phi_0, \tag{6.2}$$

respectively. The electric charges of up and down quarks, $q_{\rm u} = 2e/3$ and $q_{\rm d} = -e/3$, respectively, determine the magnetizations $\boldsymbol{M}_{\rm u}$ and $\boldsymbol{M}_{\rm d}$, respectively, for the NA-CSLs, which are anti-parallel with different magnitudes and have a net magnetization, referred to as ferrimagnetism. For the η-CSL, the magnetizations become parallel as $\boldsymbol{M}_\eta$, implying ferromagnetism. Hence, S_1 (ℓ_1) in figure 3(c) [(d)] is a critical velocity (lattice size) separating ferrimagnetic and ferromagnetic magnetizations. Because rotation induces magnetization, this is a type of inverse gyromagnetic effect, called the Barnett effect. This magnetism of the η-CSL is specific to two-flavor quarks and does not exist in three-flavor quarks, [18] where the $\mathrm{U(1)_A}$ meson is called η' (see also [17]).

7 Concluding remark

Let us first discuss the possibility of realization of the NA-CSL in non-central heavy ion collision experiments. The largest vorticity of the current experiment has a magnitude of the order of 10^{22}/s [1, 2].

On the other hand, the critical rotation velocity of the η-CSL for three flavor was estimated to be larger by one order of magnitude [18]. In this work we have shown that the critical rotation velocity of the NA-CSL is smaller than that of the η-CSL in the most parametric regions. Although our results are shown for the two-flavor case, the crucial point is including the pion's degrees of freedom. Hence, our results are, at least qualitatively, correct for the three-flavor case. Therefore we expect that realizing the NA-CSLs experimentally is in general easier than the η-CSLs.We also point out that the low-energy heavy ion collision experiments would be more suitable to find the NA-CSLs. The low-energy collisions would produce compressed matter because nucleons stay at the collision point. Moreover, the $\Lambda(\bar{\Lambda})$ hyperon polarization increases as the collision energy $\sqrt{s}$ decreases, indicating increase of the angular velocity [1, 2]. Thus, the NA-CSL may be reached in the near future low-energy heavy ion collision experiments.

[7] See appendix B for the derivations of the linearized EOMs for the NA-CSL and the gapless modes.

[8] d is also a gapless mode called a quasi-NG mode, however, this is peculiar for $\beta = \epsilon = 0$. In general, d is gapful.

JHEP08(2022)305

In this paper, we have focused on zero temperature. Of course, effects of finite temperature on the NA-CSL would be important, but before the CSLs, we have to investigate the CVE at finite temperature, which is not sufficiently understood yet and is left for future study. At this moment, we would like to emphasize that the CSL is not destroyed by the infinitesimally small thermal fluctuations due to the explicit breaking of rotational symmetry by the global rotation (see ref. [29] for a related study). In contrast, when systems have the rotational symmetry, the thermal fluctuations destroy field configurations modulating in one direction [48, 49].

Finally, we comment on the NA-CSL in quark matter at large $\mu_{\rm B}$. In the two-flavor case, the ground state without rotation is the 2SC phase [44–47]. In this phase, $\mathrm{U}(1)_{\rm A}$ symmetry is spontaneously broken, but the chiral symmetry $\mathrm{SU}(2)_{\rm R} \times \mathrm{SU}(2)_{\rm L}$ is unbroken. Hence, the NA-CSLs do not exist in the two-flavor case at asymptotically high baryon density. On the other hand, in the three-flavor case, not only $\mathrm{U}(1)_{\rm A}$ but also the chiral symmetry $\mathrm{SU}(3)_{\rm R} \times \mathrm{SU}(3)_{\rm L}$ is spontaneously broken in the color-flavor locked phase, which is the ground state in three flavor case without rotation [50]. At the large $\mu_{\rm B}$ region, the instanton effect is suppressed due to the Debye screening [51, 52], leading to the small β. This implies that the confining η'-CSL phase tends to be suppressed whereas the NA-CSL phases would dominate in the phase digram. It would be interesting to extend our two-flavor study to the three-flavor one.

Acknowledgments

This work is supported in part by the JSPS Grant-in-Aid for Scientific Research (KAKENHI Grant No. JP22H01221 (M.E. and M.N.), No. JP19K03839 (M.E.), No. JP18H01217 (M.N.) and No. JP21H01084 (K.N.)). It is also supported by the MEXT KAKENHI Grant-in-Aid for Scientific Research on Innovative Areas "Discrete Geometric Analysis for Materials Design" No. JP17H06462 (M.E.) from the MEXT of Japan. K. N. is supported by JSPS KAKENHI Grant No. 19J21593.

A Some formulae for chiral Lagrangian under rotation

Here, we summarize rotational effects on the chiral Lagrangian. The metric in the rotating frame around the z-axis is given by

$$g_{\mu\nu} = \begin{pmatrix} 1-\Omega^2(x^2+y^2) & \Omega y & -\Omega x & 0 \\ \Omega y & -1 & 0 & 0 \\ -\Omega x & 0 & -1 & 0 \\ 0 & 0 & 0 & -1 \end{pmatrix}, \tag{A.1}$$

where Ω is the angular velocity. In addition, the rotation effect appears via the chiral vortical effect (CVE), which is represented in the chiral Lagrangian [17, 18] by

$$\mathcal{L}_{\rm CVE} = \frac{N_c}{4\pi^2}\mu_b\mu_c\left(d_{Abc}\,\boldsymbol{\Omega}\cdot\boldsymbol{\nabla}\frac{\pi_A}{f_\pi} + d_{0bc}\,\boldsymbol{\Omega}\cdot\boldsymbol{\nabla}\frac{\eta}{f_\eta}\right) = \frac{\Omega}{2\pi^2 N_c}\mu_B^2\partial_z\frac{\eta}{f_\eta} \tag{A.2}$$

JHEP08(2022)305

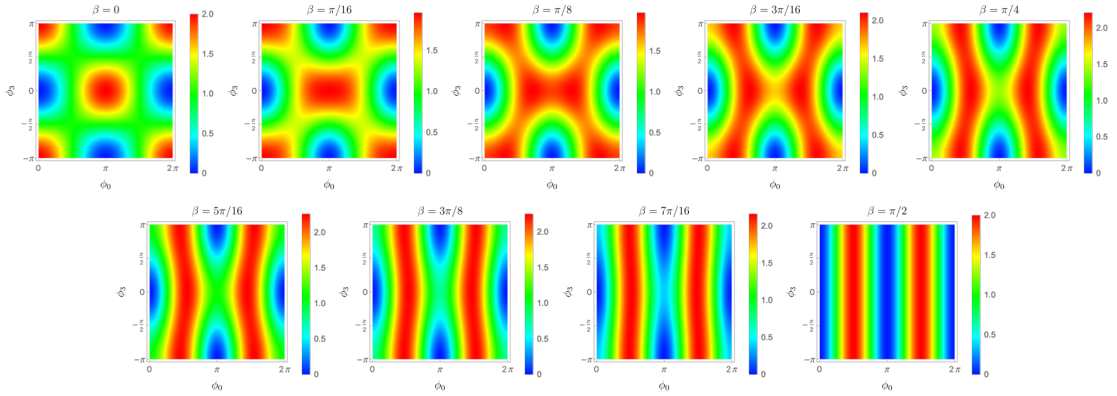

Figure 4. The scalar potential $V(\phi_0, \phi_3; \beta)$ in the ϕ_0-ϕ_3 plane ($\phi_0 \in [0, 2\pi]$ and $\phi_3 \in [-\pi, \pi]$) for $\beta = 0, \pi/16, \cdots, \pi/2$. The colors show the potential hight as indicated by the color bars.

with $d_{abc} = \frac{1}{2}\mathrm{Tr}\left[\lambda_a \{\lambda_b, \lambda_c\}\right]$ (a = 0, 1, 2, 3), and at the rightmost equality, $\mu_A = 0$ ($A = 1, 2, 3$), and the zeroth component $\mu_0 = \mu_\mathrm{B}/N_c$, which is valid for baryonic matter, are set. The CVE term in eq. (A.2) is used in eq. (1) of the the main text.

Next, we explain the scalar potential in the chiral Lagrangian studied in the main text. The dimensionless scalar potential for ϕ_0 and ϕ_3 appearing in the Hamiltonian $C^{-1}\mathcal{H}$ can be parametrized by β defined by $\tan\beta = A/(4mB)$ as

$$V(\phi_0, \phi_3; \beta) = \sin\beta(1 - \cos 2\phi_0) + \cos\beta(1 - \cos\phi_0 \cos\phi_3). \tag{A.3}$$

This is bounded from below as $V \geq 0$. Note that the case of $\beta = 0$ corresponds to the limit where the anomaly term is ignored, and the case of $\beta = \pi/2$ corresponds to the chiral limit where the quark mass terms are absent. Except for the chiral limit, the potential minima are placed at $(\phi_0, \phi_3) = (2m\pi, 2n\pi)$ and $((2m+1)\pi, (2n+1)\pi)$ for $m, n \in \mathbb{Z}$, as shown in figure 4. All of them identically correspond to the unique vacuum in terms of the U(2) field U: $U = \mathbf{1}_2$. The chiral limit $\beta = \pi/2$ for which the potential V does not depend on ϕ_3 reflecting the fact that the Lagrangian is invariant under the full chiral symmetry $U \to V_L^\dagger U V_R$. This is explicitly broken to the vector symmetry $V_L = V_R$ by the mass term for $\beta \neq \pi/2$.

The equations of motion for $\phi_{0,3}$ under the assumption that $\phi_{0,3}$ is static and depends only on ζ read

$$\phi_0'' - \frac{\cos\beta}{2}\left(\sin(\phi_0 + \phi_3) + \sin(\phi_0 - \phi_3)\right) - 2\sin\beta\sin 2\phi_0 = 0, \tag{A.4}$$

$$(1 - \epsilon)\phi_3'' - \frac{\cos\beta}{2}\left(\sin(\phi_0 + \phi_3) - \sin(\phi_0 - \phi_3)\right) = 0, \tag{A.5}$$

where the prime denotes differentiation with respect to ζ. Note that the CVE term does not appear because it is the topological term. These are the EOMs which we solved to obtain all the background CSs and CSLs configurations in the main text.

Note that $\phi_3 = 0$ solves eq. (A.5), and eq. (A.4) reduces to

$$\phi_0'' - \cos\beta\sin\phi_0 - 2\sin\beta\sin 2\phi_0 = 0. \tag{A.6}$$

JHEP08(2022)305

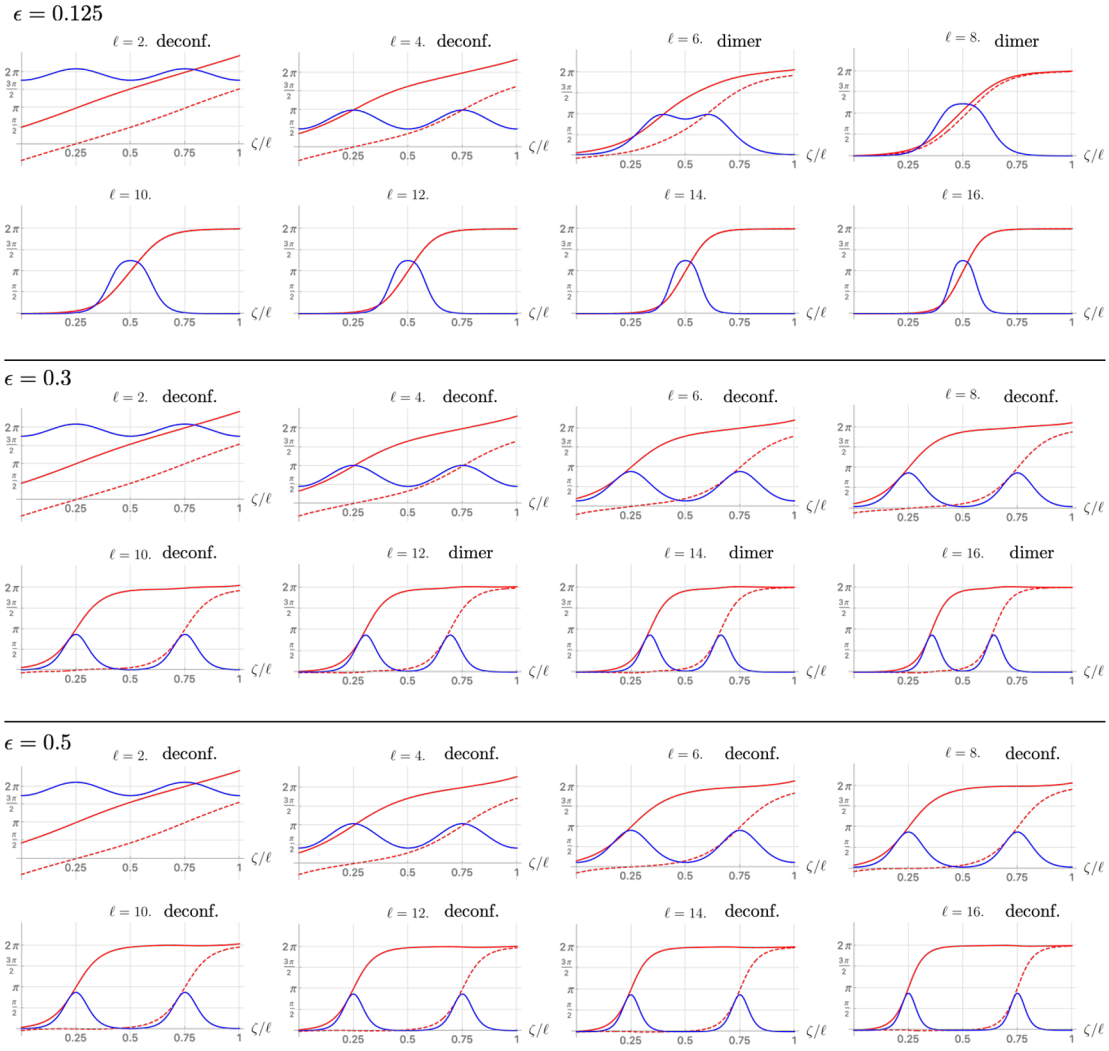

Figure 5. The numerical solutions of CSLs with the fixed $\beta = \pi/16$. The solutions in the top/middle/bottom row are for ϵ =0.125/0.3/0.5, respectively. For each ϵ we show the CSL with the lattice space $\ell = 2, 4, 6, 8, 10, 12, 14, 16$. The horizontal axes is normalized coordinate ζ/ℓ, and the red-solid and red-dashed curves show ϕ_+ and ϕ_-, respectively. The blue-solid curve correspond to the energy density. We put "deconf." if the CSL is in the deconfinement phase, and "dimer" if it is in the dimer phase.

The second and third terms have different periodicities 2π and π with respect to ϕ_0, and the above equation is the so-called double sine-Gordon equations in the literature [56, 57]. However, solutions (η-CS and η-CSL) with $\phi_3 = 0$ are not necessarily stable because the pions can be tachyonic for some parameter regions, as explained in the main text.

In figure 5 we show three typical series of CSLs with β fixed as $\beta = \pi/16$, whereas ϵ is varied as $\epsilon = 0.125$, 0.3, and 0.5. As we explain in the main text, β and $\epsilon(> 0)$ yield attractive and repulsive forces between u-CS and d-CS, respectively. The repulsive force for $\epsilon = 0.125$ is relatively weak compared with the attractive force at $\beta = \pi/16$, so that the CSL with sufficiently large period ℓ is an η-CSL in the confining phase. As the period

JHEP08(2022)305

ℓ decreases, the CSL enters in the dimer phase, and finally goes into the deconfing phase. The repulsive force of $\epsilon = 0.3$ is stronger than that of $\epsilon = 0.125$, so that the CSL at the large lattice size ℓ is not the η-CSL but the dimer NA-CSL. When ϵ is further large, $\epsilon = 0.5$, the repulsive force always dominates and the CSL is always in the deconfining phase. These solutions are used for obtaining figure 3 in the main text.

B Derivation of Linearized EOMs around the backgrounds

Here we derive linearized EOMs for linear perturbations around background solutions. Let $\bar{\phi}_0$ and $\bar{\phi}_3$ be a solution to eqs. (A.4) and (A.5) with $\bar{\phi}_1 = \pi_1/f_\pi = 0$ and $\bar{\phi}_2 = \pi_2/f_\pi = 0$.

Consider the derivation of linearized equations of motion for small fluctuations:

$$\phi_{0,3} = \bar{\phi}_{0,3}(\zeta) + \delta\phi_{0,3}, \quad \phi_{1,2} = \delta\phi_{1,2}. \tag{B.1}$$

For the zeroth and third components, we find

$$\left[\partial^2 + \begin{pmatrix} 4\sin\beta\cos 2\bar{\phi}_0 + \cos\beta\cos\bar{\phi}_0\cos\bar{\phi}_3 & -\cos\beta\sin\bar{\phi}_0\sin\bar{\phi}_3 \\ \frac{-\cos\beta\sin\bar{\phi}_0\sin\bar{\phi}_3}{1-\epsilon} & \frac{\cos\beta\cos\bar{\phi}_0\cos\bar{\phi}_3}{1-\epsilon} \end{pmatrix}\right]\begin{pmatrix}\delta\phi_0\\ \delta\phi_3\end{pmatrix} = 0. \tag{B.2}$$

In some cases, it is useful to change the basis by

$$\bar{\phi}_\pm = \bar{\phi}_0 \pm \bar{\phi}_3, \quad \delta\phi_\pm = \delta\phi_0 \pm \delta\phi_3. \tag{B.3}$$

In terms of the new basis, the linearized equations are expressed as

$$\left[\partial^2 + \begin{pmatrix} 2\sin\beta\cos 2\bar{\phi}_0 + \frac{2-\epsilon}{2(1-\epsilon)}\cos\beta\cos\bar{\phi}_+ & 2\sin\beta\cos 2\bar{\phi}_0 - \frac{\epsilon}{2(1-\epsilon)}\cos\beta\cos\bar{\phi}_- \\ 2\sin\beta\cos 2\bar{\phi}_0 - \frac{\epsilon}{2(1-\epsilon)}\cos\beta\cos\bar{\phi}_+ & 2\sin\beta\cos 2\bar{\phi}_0 + \frac{2-\epsilon}{2(1-\epsilon)}\cos\beta\cos\bar{\phi}_- \end{pmatrix}\right]\begin{pmatrix}\delta\phi_+\\ \delta\phi_-\end{pmatrix} = 0. \tag{B.4}$$

To obtain the linearized equations for $\delta\phi_{1,2}$, it is useful to modify the variables as $\delta\pi_\pm = \delta\phi_1 \pm i\delta\phi_2$. The resulting equations are decoupled as

$$\left[(1-\epsilon)\left(\partial^2 + 2i\bar{\phi}_3'\partial_\zeta - i(\bar{\phi}_3')^2\right) + \cos\beta\cos\bar{\phi}_0\cos\bar{\phi}_3\right]\delta\pi_\pm = 0. \tag{B.5}$$

The kinetic term can be canonicalized by

$$\delta\tilde{\pi}_\pm = e^{\mp i\bar{\phi}_3}\delta\pi_\pm, \tag{B.6}$$

and we obtain

$$\left[\partial^2 - (\bar{\phi}_3')^2 + \frac{\cos\beta}{1-\epsilon}\cos\bar{\phi}_0\cos\bar{\phi}_3\right]\delta\tilde{\pi}_\pm = 0. \tag{B.7}$$

Thus, $\delta\phi_{0,3}$ ($\delta\phi_\pm$) are mixed to each other, while $\delta\tilde{\pi}_\pm$ are isolated.

B.1 η-CSL

When the background solution is the η-CSL, $\bar{\phi}_3 = 0$, the above linearized EOMs reduce to

$$\left[\partial^2 + \begin{pmatrix} 4\sin\beta\cos 2\bar{\phi}_0 + \cos\beta\cos\bar{\phi}_0 & 0 \\ 0 & \frac{\cos\beta\cos\bar{\phi}_0}{1-\epsilon} \end{pmatrix}\right]\begin{pmatrix}\delta\phi_0\\ \delta\phi_3\end{pmatrix} = 0, \tag{B.8}$$

$$\left(\partial^2 + \frac{\cos\beta\cos\bar{\phi}_0}{1-\epsilon}\right)\delta\pi_\pm = 0. \tag{B.9}$$

JHEP08(2022)305

Note that $\delta\phi_3$ and $\delta\pi_\pm = \delta\tilde{\pi}_\pm\big|_{\bar{\phi}_3=0}$ satisfy the identical equations, which is expected from the fact that the $\mathrm{SU}(2)_\mathrm{V}$ symmetry is kept by the η-CSL. Note that $\delta\phi_0$ is decoupled from the others, and its linearized EOM is identical to that of the double sine-Gordon equation. Therefore, no tachyonic instabilities arise in the $\delta\phi_0$ sector. The lowest eigenstate is the translational NG mode whose eigenvalue is exactly zero.

On the other hand, the stability in the pion sector can be analyzed by the Schrödinger-like equation

$$\left(-\frac{d^2}{d\zeta^2} + \frac{\cos\beta\cos\bar{\phi}_0}{1-\epsilon}\right)\psi_n = m_n^2\psi_n. \tag{B.10}$$

The linear stability of the η-CSL can be clarified by obtaining mass square eigenvalues: if the lowest eigenvalue is zero or positive (negative), the η-CSL is (un)stable against local fluctuations. We thus obtain a part of figure 2 (a) and (b) and figure 3 (c) and (d) in the main text.

B.2 NA-CSL at $\beta = \epsilon = 0$

Here, we study the stability of NA-CSLs for the special case $\beta = \epsilon = 0$, where the up-CSL and down-CSL do not interact. This can be easily seen by rewriting the Hamiltonian in terms of $\phi_\pm = \phi_0 \pm \phi_3$. It is merely a sum of two sine-Gordon Hamiltonians: $\mathcal{H} = \mathcal{H}_+ + \mathcal{H}_-$ with

$$C^{-1}\mathcal{H}_\pm = \frac{1}{2}\left\{\frac{1}{2}\left(\frac{d\phi_\pm}{d\zeta}\right)^2 + 1 - \cos\phi_\pm - S\frac{d\phi_\pm}{d\zeta}\right\}, \tag{B.11}$$

and the Schrödinger-like equations are

$$\left(-\frac{d^2}{d\zeta^2} + \cos\bar{\phi}_\pm\right)\delta\phi_{\pm,n} = m_{\pm,n}^2\delta\phi_{\pm,n}, \tag{B.12}$$

$$\left(-\frac{d^2}{d\zeta^2} - (\bar{\phi}_3')^2 + \cos\bar{\phi}_0\cos\bar{\phi}_3\right)\delta\tilde{\pi}_{\pm,n} = \tilde{m}_{\pm,n}^2\delta\tilde{\pi}_{\pm,n}. \tag{B.13}$$

Let us consider a background CSL with the u- and d-CSLs with the separation d as

$$\bar{\phi}_+ = 2\,\mathrm{am}\left(\frac{\zeta - d/2}{k}, k\right) + \pi, \quad \bar{\phi}_- = 2\,\mathrm{am}\left(\frac{\zeta + d/2}{k}, k\right) + \pi, \tag{B.14}$$

where $\mathrm{am}(z,k)$ denotes the Jacobi's amplitude function and k is the elliptic modulus between $0 \le k \le 1$. The $\delta\phi_-$-sector is a copy of the $\delta\phi_+$-sector, and they are identical to the linearized EOM of the well-known sine-Gordon soliton. Therefore, we immediately find that the lowest eigenstate is massless as

$$(m_{\pm,0})^2 = 0, \quad \delta\phi_{\pm,0} = \mathrm{dn}\left(\frac{\zeta \mp d/2}{k}, k\right). \tag{B.15}$$

These two are the independent phonons propagating on the u- and d-CSLs. The overall translation is the usual translational zero mode, while the separation d between them

JHEP08(2022)305

corresponds to the so-called quasi-NG mode.[9] This appears for the non-interactive case $\beta = \epsilon = 0$ and becomes gapped in the general case.

On the other hand, the Schrödinger potential for $\delta\tilde{\pi}_\pm$ is more complicated. It can be explicitly written as

$$-(\bar{\phi}_3')^2 + \cos\bar{\phi}_0 \cos\bar{\phi}_3 = -\frac{1}{k^2}\left(\mathrm{dn}_+ - \mathrm{dn}_-\right)^2 - \mathrm{cn}_+^2\mathrm{cn}_-^2 + \mathrm{sn}_+^2\mathrm{sn}_-^2, \tag{B.16}$$

with $\mathrm{dn}_\pm = \mathrm{dn}\left(\frac{\zeta \pm d/2}{k}, k\right)$, and similar to cn and sn, where dn, cn and sn are the Jacobi's elliptic functions; the delta amplitude, the elliptic cosine, and the elliptic sine, respectively. We find that the lowest eigenvalues are zero and the corresponding mode functions are given by

$$(\tilde{m}_{\pm,0})^2 = 0, \quad \delta\tilde{\pi}_{\pm,0} = \mathrm{dn}\left(\frac{\zeta - d/2}{k}, k\right) + \mathrm{dn}\left(\frac{\zeta + d/2}{k}, k\right). \tag{B.17}$$

These correspond to the gapless NG modes, isospinons explained in the main text, associated with the symmetry breaking $\mathrm{SU}(2)_\mathrm{V} \to \mathrm{U}(1)$ in the presence of the NA-CSL. These isospinons are type-A NG modes having linear dispersion relations in the classification of NG modes [58–60] since they are antiffero. While NA NG modes propagating on a NA vortex lattice are known [61], those on a soliton (domain wall) lattice found in this Letter are new.

References

[1] STAR collaboration, *Global Λ hyperon polarization in nuclear collisions: evidence for the most vortical fluid*, *Nature* **548** (2017) 62 [arXiv:1701.06657] [INSPIRE].

[2] STAR collaboration, *Global polarization of Λ hyperons in Au+Au collisions at* $\sqrt{s_{NN}} = 200$ *GeV*, *Phys. Rev. C* **98** (2018) 014910 [arXiv:1805.04400] [INSPIRE].

[3] LIGO Scientific and Virgo collaborations, *GW170817: observation of gravitational waves from a binary neutron star inspiral*, *Phys. Rev. Lett.* **119** (2017) 161101 [arXiv:1710.05832] [INSPIRE].

[4] LIGO Scientific and Virgo collaborations, *GW190425: observation of a compact binary coalescence with total mass* $\sim 3.4 M_\odot$, *Astrophys. J. Lett.* **892** (2020) L3 [arXiv:2001.01761] [INSPIRE].

[9] Quasi-NG modes are gapless modes which are not related to symmetry breaking of the whole system [53, 54]. Quasi-NG modes associated to the presence of parallel domain walls were found in ref. [55]. In this case, the exchange between NG and quasi-NG modes with keeping the total number occurs [53] when two solitons coincide. In the NA-CSL for $\beta = \epsilon = 0$, there are three NG modes (translation and isospinons) and one quasi-NG mode when the u-CSL and d-CSL are separated, while there is one NG mode (translation) and three quasi-NG modes when they coincide.

JHEP08(2022)305

[5] T.E. Riley et al., *A NICER view of PSR J0030+0451: millisecond pulsar parameter estimation*, *Astrophys. J. Lett.* **887** (2019) L21 [arXiv:1912.05702] [INSPIRE].

[6] M.C. Miller et al., *PSR J0030+0451 mass and radius from NICER data and implications for the properties of neutron star matter*, *Astrophys. J. Lett.* **887** (2019) L24 [arXiv:1912.05705] [INSPIRE].

[7] H.-L. Chen, K. Fukushima, X.-G. Huang and K. Mameda, *Analogy between rotation and density for Dirac fermions in a magnetic field*, *Phys. Rev. D* **93** (2016) 104052 [arXiv:1512.08974] [INSPIRE].

[8] S. Ebihara, K. Fukushima and K. Mameda, *Boundary effects and gapped dispersion in rotating fermionic matter*, *Phys. Lett. B* **764** (2017) 94 [arXiv:1608.00336] [INSPIRE].

[9] Y. Jiang and J. Liao, *Pairing phase transitions of matter under rotation*, *Phys. Rev. Lett.* **117** (2016) 192302 [arXiv:1606.03808] [INSPIRE].

[10] M.N. Chernodub and S. Gongyo, *Interacting fermions in rotation: chiral symmetry restoration, moment of inertia and thermodynamics*, *JHEP* **01** (2017) 136 [arXiv:1611.02598] [INSPIRE].

[11] M.N. Chernodub and S. Gongyo, *Effects of rotation and boundaries on chiral symmetry breaking of relativistic fermions*, *Phys. Rev. D* **95** (2017) 096006 [arXiv:1702.08266] [INSPIRE].

[12] Y. Liu and I. Zahed, *Rotating Dirac fermions in a magnetic field in* $1+2$ *and* $1+3$ *dimensions*, *Phys. Rev. D* **98** (2018) 014017 [arXiv:1710.02895] [INSPIRE].

[13] H. Zhang, D. Hou and J. Liao, *Mesonic condensation in isospin matter under rotation*, *Chin. Phys. C* **44** (2020) 111001 [arXiv:1812.11787] [INSPIRE].

[14] L. Wang, Y. Jiang, L. He and P. Zhuang, *Local suppression and enhancement of the pairing condensate under rotation*, *Phys. Rev. C* **100** (2019) 034902 [arXiv:1901.00804] [INSPIRE].

[15] H.-L. Chen, X.-G. Huang and K. Mameda, *Do charged pions condense in a magnetic field with rotation?*, arXiv:1910.02700 [INSPIRE].

[16] H.-L. Chen, X.-G. Huang and J. Liao, *QCD phase structure under rotation*, *Lect. Notes Phys.* **987** (2021) 349 [arXiv:2108.00586] [INSPIRE].

[17] X.-G. Huang, K. Nishimura and N. Yamamoto, *Anomalous effects of dense matter under rotation*, *JHEP* **02** (2018) 069 [arXiv:1711.02190] [INSPIRE].

[18] K. Nishimura and N. Yamamoto, *Topological term, QCD anomaly, and the* η' *chiral soliton lattice in rotating baryonic matter*, *JHEP* **07** (2020) 196 [arXiv:2003.13945] [INSPIRE].

[19] A. Vilenkin, *Macroscopic parity violating effects: neutrino fluxes from rotating black holes and in rotating thermal radiation*, *Phys. Rev. D* **20** (1979) 1807 [INSPIRE].

[20] A. Vilenkin, *Quantum field theory at finite temperature in a rotating system*, *Phys. Rev. D* **21** (1980) 2260 [INSPIRE].

[21] D.T. Son and P. Surowka, *Hydrodynamics with triangle anomalies*, *Phys. Rev. Lett.* **103** (2009) 191601 [arXiv:0906.5044] [INSPIRE].

[22] K. Landsteiner, E. Megias and F. Pena-Benitez, *Gravitational anomaly and transport*, *Phys. Rev. Lett.* **107** (2011) 021601 [arXiv:1103.5006] [INSPIRE].

[23] K. Landsteiner, E. Megias and F. Pena-Benitez, *Anomalous transport from Kubo formulae*, *Lect. Notes Phys.* **871** (2013) 433 [arXiv:1207.5808] [INSPIRE].

JHEP08(2022)305

[24] K. Landsteiner, *Notes on anomaly induced transport*, *Acta Phys. Polon. B* **47** (2016) 2617 [arXiv:1610.04413] [INSPIRE].

[25] D.T. Son and M.A. Stephanov, *Axial anomaly and magnetism of nuclear and quark matter*, *Phys. Rev. D* **77** (2008) 014021 [arXiv:0710.1084] [INSPIRE].

[26] M. Eto, K. Hashimoto and T. Hatsuda, *Ferromagnetic neutron stars: axial anomaly, dense neutron matter, and pionic wall*, *Phys. Rev. D* **88** (2013) 081701 [arXiv:1209.4814] [INSPIRE].

[27] T. Brauner and N. Yamamoto, *Chiral soliton lattice and charged pion condensation in strong magnetic fields*, *JHEP* **04** (2017) 132 [arXiv:1609.05213] [INSPIRE].

[28] S. Chen, K. Fukushima and Z. Qiu, *Skyrmions in a magnetic field and $\pi 0$ domain wall formation in dense nuclear matter*, *Phys. Rev. D* **105** (2022) L011502 [arXiv:2104.11482] [INSPIRE].

[29] T. Brauner and S.V. Kadam, *Anomalous low-temperature thermodynamics of QCD in strong magnetic fields*, *JHEP* **11** (2017) 103 [arXiv:1706.04514] [INSPIRE].

[30] T. Brauner and S. Kadam, *Anomalous electrodynamics of neutral pion matter in strong magnetic fields*, *JHEP* **03** (2017) 015 [arXiv:1701.06793] [INSPIRE].

[31] T. Brauner, H. Kolešová and N. Yamamoto, *Chiral soliton lattice phase in warm QCD*, *Phys. Lett. B* **823** (2021) 136767 [arXiv:2108.10044] [INSPIRE].

[32] A. Yamada and N. Yamamoto, *Floquet vacuum engineering: laser-driven chiral soliton lattice in the QCD vacuum*, *Phys. Rev. D* **104** (2021) 054041 [arXiv:2107.07074] [INSPIRE].

[33] T. Brauner, G. Filios and H. Kolešová, *Chiral soliton lattice in QCD-like theories*, *JHEP* **12** (2019) 029 [arXiv:1905.11409] [INSPIRE].

[34] T. Brauner, G. Filios and H. Kolešová, *Anomaly-induced inhomogeneous phase in quark matter without the sign problem*, *Phys. Rev. Lett.* **123** (2019) 012001 [arXiv:1902.07522] [INSPIRE].

[35] I.E. Dzyaloshinsky, *Theory of helicoidal structures in antiferromagnets. I. Nonmetals*, *Sov. Phys. JETP* **19** (1964) 960.

[36] Y. Togawa et al., *Chiral magnetic soliton lattice on a chiral helimagnet*, *Phys. Rev. Lett.* **108** (2012) 107202.

[37] Y. Togawa, Y. Kousaka, K. Inoue and J.I. Kishine, *Symmetry, structure, and dynamics of monoaxial chiral magnets*, *J. Phys. Soc. Jpn.* **85** (2016) 112001.

[38] M. Eto and M. Nitta, *Quantum nucleation of topological solitons*, to appear on *JHEP* , arXiv:2207.00211 [INSPIRE].

[39] T. Higaki, K. Kamada and K. Nishimura, *Formation of chiral soliton lattice*, arXiv:2207.00212 [INSPIRE].

[40] M. Nitta, *Non-Abelian sine-Gordon solitons*, *Nucl. Phys. B* **895** (2015) 288 [arXiv:1412.8276] [INSPIRE].

[41] M. Eto and M. Nitta, *Non-Abelian sine-Gordon Solitons: correspondence between $SU(N)$ Skyrmions and $\mathbb{C}P^{N-1}$ lumps*, *Phys. Rev. D* **91** (2015) 085044 [arXiv:1501.07038] [INSPIRE].

[42] D.T. Son and A.R. Zhitnitsky, *Quantum anomalies in dense matter*, *Phys. Rev. D* **70** (2004) 074018 [hep-ph/0405216] [INSPIRE].

JHEP08(2022)305

[43] M. Eto, Y. Hirono, M. Nitta and S. Yasui, *Vortices and other topological solitons in dense quark matter*, *PTEP* **2014** (2014) 012D01 [arXiv:1308.1535] [INSPIRE].

[44] B.C. Barrois, *Superconducting quark matter*, *Nucl. Phys. B* **129** (1977) 390.

[45] D. Bailin and A. Love, *Superfluidity and superconductivity in relativistic fermion systems*, *Phys. Rept.* **107** (1984) 325 [INSPIRE].

[46] M.G. Alford, K. Rajagopal and F. Wilczek, *QCD at finite baryon density: Nucleon droplets and color superconductivity*, *Phys. Lett. B* **422** (1998) 247 [hep-ph/9711395] [INSPIRE].

[47] R. Rapp, T. Schäfer, E.V. Shuryak and M. Velkovsky, *Diquark Bose condensates in high density matter and instantons*, *Phys. Rev. Lett.* **81** (1998) 53 [hep-ph/9711396] [INSPIRE].

[48] Y. Hidaka, K. Kamikado, T. Kanazawa and T. Noumi, *Phonons, pions and quasi-long-range order in spatially modulated chiral condensates*, *Phys. Rev. D* **92** (2015) 034003 [arXiv:1505.00848] [INSPIRE].

[49] T.-G. Lee, E. Nakano, Y. Tsue, T. Tatsumi and B. Friman, *Landau-Peierls instability in a Fulde-Ferrell type inhomogeneous chiral condensed phase*, *Phys. Rev. D* **92** (2015) 034024 [arXiv:1504.03185] [INSPIRE].

[50] M.G. Alford, K. Rajagopal and F. Wilczek, *Color flavor locking and chiral symmetry breaking in high density QCD*, *Nucl. Phys. B* **537** (1999) 443 [hep-ph/9804403] [INSPIRE].

[51] D.J. Gross, R.D. Pisarski and L.G. Yaffe, *QCD and instantons at finite temperature*, *Rev. Mod. Phys.* **53** (1981) 43 [INSPIRE].

[52] E.V. Shuryak, *The role of instantons in quantum chromodynamics. 3. Quark-gluon plasma*, *Nucl. Phys. B* **203** (1982) 140 [INSPIRE].

[53] M. Nitta, *Moduli space of global symmetry in $N = 1$ supersymmetric theories and the quasiNambu-Goldstone bosons*, *Int. J. Mod. Phys. A* **14** (1999) 2397 [hep-th/9805038] [INSPIRE].

[54] M. Nitta and D.A. Takahashi, *Quasi-Nambu-Goldstone modes in nonrelativistic systems*, *Phys. Rev. D* **91** (2015) 025018 [arXiv:1410.2391] [INSPIRE].

[55] M. Eto, T. Fujimori, M. Nitta, K. Ohashi and N. Sakai, *Domain walls with non-Abelian clouds*, *Phys. Rev. D* **77** (2008) 125008 [arXiv:0802.3135] [INSPIRE].

[56] C.A. Condat, R.A. Guyer and M.D. Miller, *Double sine-Gordon chain*, *Phys. Rev. B* **27** (1983) 474.

[57] C. Ross, N. Sakai and M. Nitta, *Exact ground states and domain walls in one dimensional chiral magnets*, *JHEP* **12** (2021) 163 [arXiv:2012.08800] [INSPIRE].

[58] H. Watanabe and H. Murayama, *Unified description of Nambu-Goldstone bosons without Lorentz invariance*, *Phys. Rev. Lett.* **108** (2012) 251602 [arXiv:1203.0609] [INSPIRE].

[59] Y. Hidaka, *Counting rule for Nambu-Goldstone modes in nonrelativistic systems*, *Phys. Rev. Lett.* **110** (2013) 091601 [arXiv:1203.1494] [INSPIRE].

[60] D.A. Takahashi and M. Nitta, *Counting rule of Nambu-Goldstone modes for internal and spacetime symmetries: Bogoliubov theory approach*, *Annals Phys.* **354** (2015) 101 [arXiv:1404.7696] [INSPIRE].

[61] M. Kobayashi, E. Nakano and M. Nitta, *Color magnetism in non-Abelian vortex matter*, *JHEP* **06** (2014) 130 [arXiv:1311.2399] [INSPIRE].

JHEP08(2022)305